JOURNAL OF MATERIALS SCIENCE 31 (1996) 3937–3943

Stability of the perovskite phase in PMN–PZN–PT ceramics

P. ESCURE, E. LATTARD, M. LEJEUNE, J. F. BAUMARD
Laboratoire de Matériaux Céramiques et traitements de Surface, URA CNRS 320, Ecole Nationale Supérieure de Céramique Industrielle, 47 à 73, Avenue Albert Thomas, 87065 Limoges Cedex, France

The thermal stability of ceramics based on PMN, PZN and their solid solutions PMN–PT, PZN–PT (PMN = $PbMg_{1/3}Nb_{2/3}O_3$, PZN = $PbZn_{1/3}Nb_{2/3}O_3$, PT = $PbTiO_3$) during sintering is investigated. The present work confirms that the incorporation of a limited excess of MgO in the starting materials is actually quite beneficial for the synthesis of a pure PMN perovskite phase, and that it prevents the formation of a secondary pyrochlore-type phase, after PbO loss during firing. An excess of ZnO is much less efficient for the stabilization of the PZN compound. Examination of the microstructural evolution as well as analysis of second phases in these materials and in their solid solutions formed with lead titanate by wavelength dispersive spectroscopy and/or energy dispersive X-ray spectroscopy techniques, allows a mechanism to be proposed for the stabilization of the PMN-based perovskite phases by an excess of MgO.

1. Introduction

Lead magnesium niobate (PMN, $PbMg_{1/3}Nb_{2/3}O_3$) is a ferroelectric material characterized by a high dielectric constant (12 000) at $-15\,^{\circ}C$ and a low sintering temperature. So, it is a promising candidate for low-price multilayer capacitors [1–3]. Moreover, as induced electrostrictive strains are proportional to the square of the dielectric constant, PMN is also interesting for electrostrictive applications [4, 5]. It has been reported that the electrostrictive strains in 0.9PMN–0.1PT ceramics are comparable to those of PZT, but in addition they are more reproducible under cycling [6].

Piezoelectric properties of PMN ceramics have also been investigated. This has concerned solid solutions of PMN ($P_S = 6\,\mu C\,cm^{-2}$ at $10\,^{\circ}C$) with PT (PT = $PbTiO_3$, $T_c = 490\,^{\circ}C$, $P_S = 750\,\mu C\,cm^{-2}$ at $23\,^{\circ}C$) and $PbZrO_3$ ($T_c = 230\,^{\circ}C$) in order to increase the Curie temperature and the spontaneous polarization of the material. Large piezoelectric coefficients, which could be improved by incorporation of substituents or additives, were obtained for compositions near the morphotropic phase boundaries [7, 8].

Recently, one of our investigations focused on the piezoelectric properties of PMN–PZN–PT ceramics (PZN = $PbZn_{1/3}Nb_{2/3}O_3$) [9–11]. The compositions selected were $(0.6 - y)$ PMN–yPZN–0.4PT with $y = 0$, 0.2, 0.4 and 0.6. The main objective of this work was to elucidate the influence of magnesium substitution by zinc on the piezoelectric properties in the vicinity of the morphotropic phase boundary [12].

During the calcination and sintering steps of these ceramics, care must be taken to avoid the formation of a pyrochlore-type phase which is detrimental to electrical properties [13]. It has been reported that the pyrochlore phase could be avoided in PMN ceramics by addition of excess MgO (≈ 5 mol%) both in the conventional mixed oxide route [14, 15] or in a columbite type process [16, 17]. As far as PZN ceramics are concerned, the perovskite phase is usually stabilized by addition of stable perovskite compounds such as $PbTiO_3$ (25 mol%), $BaTiO_3$ (7 mol%) or $SrTiO_3$ (10 mol%) [18–21]. According to these results, the perovskite phases corresponding to $(0.6 - y)$ PMN–yPZN–0.4PT should be stable owing to their large content of $PbTiO_3$.

However, one of our previous studies pointed out that a pyrochlore phase was present in $(1 - x)$ PMN–xPT ceramics with $0 < x < 0.5$ [17]. This is the reason why an excess of 6 mol% excess MgO/ZnO, balanced according to the substitution rate y, was added to the different compositions $(0.6 - y)$ PMN–yPZN–0.04PT in order to improve the formation and the stability of the perovskite phase. In previous publications [9, 10] we have shown that perovskite contents larger than 95 vol% could be reached by adjusting the temperature of calcination treatment according to the substitution rate y.

The purpose of this present work was to investigate the stability of the perovskite phase in the PMN–PZN–PT ceramics during sintering, and specifically with respect to the effect of magnesium substitution by zinc. A mechanism of perovskite to pyrochlore conversion will be proposed.

2. Experimental procedure

Different compositions were prepared from appropriate amounts of reagent-grade PbO (Merck (7401)

0022–2461

$d_{50} = 25\ \mu m$, $S_{BET} = 0.2\ m^2\ g^{-1}$), MgO (Lambert Rivière (lèger) $d_{50} = 6\ \mu m$, $S_{BET} = 27\ m^2\ g^{-1}$), ZnO (Vieille Montagne (Neige) $d_{50} = 0.3\ \mu m$, $S_{BET} = 4\ m^2\ g^{-1}$), Nb_2O_5 (Hermann and Starck (Ceramic Grade) $d_{50} = 0.4\ \mu m$, $S_{BET} = 8\ m^2\ g^{-1}$) and TiO_2 (Toho $d_{50} = 1.3\ \mu m$, $S_{BET} = 2.5\ m^2\ g^{-1}$) which were mixed by attrition milling in distilled water for 2 h with zirconia balls and a dispersant (Dolapix, PC 33-Zimmer and Schwartz). The mixtures were calcined for 3 h at selected temperatures [10, 11], then crushed and attrition milled with a binder (PVA + PEG). Discs, 16 mm diameter and 2 mm thick, were formed by uniaxial pressing at 150 MPa. Pellets, placed in a covered alumina crucible, were debinded by slow heating from room temperature to 500 °C at 100 °C h^{-1}, then buried into alumina powder to minimize PbO losses [16] and sintered between 1000 and 1200 °C for 3 h.

X-ray diffractometer scans were carried out on powders obtained by crushing the sintered samples. The relative amounts of perovskite and pyrochlore phases were calculated from the ratio of the (1 1 0) perovskite peak and the (2 2 2) pyrochlore peak intensities.

The theoretical densities of ceramics were then calculated from the relative amounts of phases, and relative densities were deduced from experimental densities.

The PbO deficiency of every composition was determined from the cumulated weight losses during calcination and sintering steps, corrected from the weight of organics.

Furthermore, polished sections corresponding to successive zones from the surface to the centre of the different sintered samples, were analysed (i) by X-ray diffraction to determine the relative amount of the pyrochlore phase, (ii) with a scanning electron microscope (Hitachi S 2500), equipped with an energy dispersive X-ray spectroscopy (EDS) detector (Kevex Delta), (iii) with a wavelength-dispersive spectroscopy (WDS) electron microprobe (Camebax Micro-Cameca). In fact, the composition of the perovskite and pyrochlore phases was determined quantitatively by WDS analysis which is more appropriate in this case than EDS because of the better split of lead and niobium signals on the WDS spectra. However, the EDS analysis was necessary to locate and identify the different inclusions in the samples, because the quality of images was better than by WDS analysis.

Moreover, after ion-beam milling, some samples were examined in a transmission electron microscope equipped with an energy dispersive X-ray detector (Jeol 2010/Link).

3. Results and discussion

3.1. Microstructural characteristics of sintered samples

The relative density, the perovskite content and the PbO deficiency of the different samples after sintering are summarized in Table I. It appears that for the same sintering temperature, the stability of the perovskite phase is better at lower ZnO contents. Conversely, the materials seem to be stable up to a larger PbO deficiency. For example, if the PbO deficiency amounts to −4 mol%, a pure perovskite phase is obtained for $y = 0$ (0.6PMN–0.4PT–0.06MgO) while 16 vol% pyrochlore phase is present for $y = 0.6$ (0.6PZN–0.4PT–0.06ZnO). As a consequence, it is difficult to obtain pyrochlore-free and densified samples at large ZnO content. So, compositions $y = 0.4$ and $y = 0.6$, sintered at lower temperatures, exhibit a very limited grain growth compared to other compositions (Fig. 1). According to these results, it appears that the stability of the PMN–PZN–PT compositions depends on the ZnO content. This confirms the lower stability of PZN compound compared to PMN, a fact which has been previously reported [22].

The aim of this work was to understand how the substitution of magnesium oxide by zinc oxide in 0.6PMN–0.4PT–0.06MgO composition affects the stability of the material and consequently the mechanism of perovskite to pyrochlore transformation. Therefore, appropriate samples were selected from among those presented in Table I, e.g. $y = 0$/1200 °C/3 h (sample 4) and $y = 0.6$/1100 °C/3 h (sample 5). Moreover, due to the numerous constituents of these

TABLE I The volume fraction of perovskite, the PbO deficiency and the relative density of $(0.6 - y)$PMN–yPZN–0.4PT–$(0.06 - z)$MgO–zZnO (with $z = y/10$) sintered at (a) 1000 °C, (b) 1100 °C, (c) 1200 °C for 3 h

y	Perovskite (vol %) ±1%	PbO deficiency (mol %) ±0.2%	Relative density ±0.5%
0	(a) 100	− 2.8	62
	(b) 100	− 3.1	92
	(c) 100	− 4.1	95 (sample 4)
0.2	100	− 1.4	83
	100	− 1.7	93
	100	− 5.3	94
0.4	100	− 2	79
	98	− 2.6	97
	–	–	–
0.6	94	− 1.6	91
	84	− 4	96 (sample 5)
	–	–	–

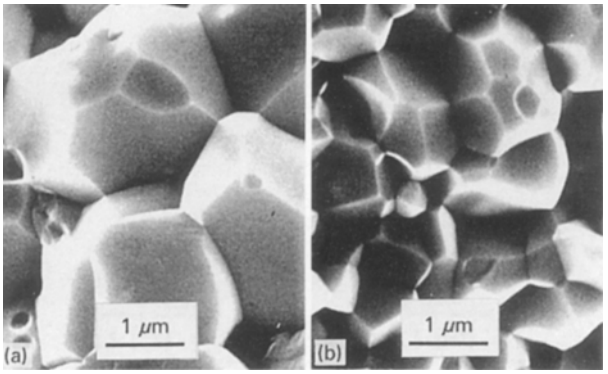

Figure 1 SEM images of fracture surfaces of samples (a) $y = 0$ sintered at 1200 °C/3 h, (b) $y = 0.6$ sintered at 1100 °C/3 h.

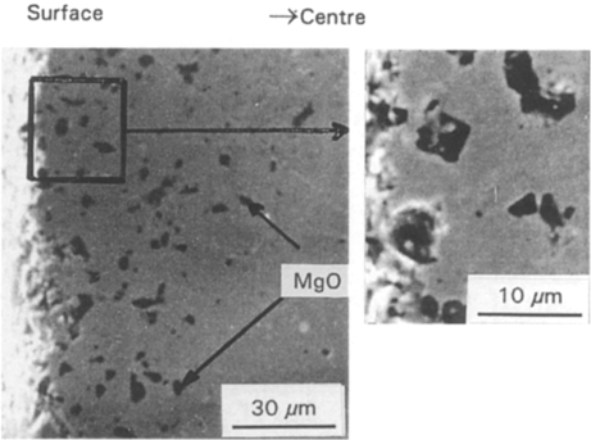

Figure 2 Polished cross-sections of a stoichiometric PMN (sample 1).

selected compositions, our study has deliberately considered PMN compositions that (i) are stoichiometric, sintered at 1200 °C for 1 h (sample 2) or 3 h (sample 1), and (ii) contain 6 mol% excess of MgO, sintered at 1200 °C for 1 h (sample 3).

Table II presents the relative amounts of perovskite phase and the PbO deficiency of these materials. As the sintered samples 2–5 are characterized by the same PbO deficiency (−4 mol%), their corresponding perovskite contents allow us to point out the influence on the perovskite stability of (i) the MgO excess by comparing samples 2 and 3, and (ii) the nature of the B site-cation (Mg^{2+} or Zn^{2+}) in the perovskite structure ABO_3 by comparing samples 4 and 5.

3.2. Characterization of polished sections of samples 1–5

3.2.1. Stoichiometric PMN samples (1 and 2)

X-ray and SEM analysis of polished sections of stoichiometric PMN materials (1 and 2) reveal a highly inhomogeneous phase distribution. Near the surface of the samples, at a depth of 20 μm (sample 2) to 200 μm (sample 1), a pyrochlore phase coexists with MgO inclusions, the number of which decreases progressively from the surface to the centre (Fig. 2). The composition of the pyrochlore phase determined by WDS was found to be $Pb_{2.01 \pm 0.02}Mg_{0.33 \pm 0.04}Nb_{1.66 \pm 0.04}O_{6.52 \pm 0.04}$. It corresponds to a 1/6 substitution of niobium ions on the B-sites by magnesium in $Pb_2Nb_2O_7$ which leads to $Pb_6(MgNb_5)O_{19.5}$. This formula is in fair agreement with those proposed previously by several authors [13, 23–25].

In the centre of the samples, the perovskite phase only is detected, with the composition $Pb_{1.06 \pm 0.03}Mg_{0.31 \pm 0.04}Nb_{0.64 \pm 0.02}O_3$. The comparison of the Mg/Nb and Pb/Nb ratios of perovskite and pyrochlore phases (Table III) shows that the pyrochlore phase has lower Mg/Nb and Pb/Nb ratios, as reported by Wang and Schulze [17].

Consequently, according to these results, the transformation of the perovskite phase to the pyrochlore phase corresponds to the following reaction:

perovskite phase → pyrochlore phase + MgO inclusions + PbO volatilized (1)

For PMN ceramics, a similar mechanism was proposed by Chen and Harmer (13), but they mention a "lead-rich intergranular phase", suggesting that lead oxide does not volatilize, but remains in the material microstructure as a glassy phase, which has been identified by Goo *et al.* [25]. In our case, no amorphous compound including lead oxide and associated with the pyrochlore phase was detected near the the surface. Moreover, the precipitation mechanism of an oxide issued from one of the perovskite B-cations (here Mg^{2+}), was previously reported for similar perovskites such as PZT, where ZrO_2 precipitation was observed [26].

3.2.2. PMN-type samples containing excess MgO (3 and 4)

No pyrochlore phase was detected by X-ray diffraction at the surface of PMN–0.06MgO (sample 3) and 0.6PMN–0.4PT–0.06MgO (sample 4). Therefore, as the PbO deficiency (−4 mol%) of samples 3 and 4 is the same as in stoichiometric sample 2 of PMN

TABLE II The volume fraction of perovskite and the PbO deficiency of samples 1–5.

samples	perovskite (vol%) ±1%	PbO deficiency (mol%) ± 0.2%
(1) Stochiometric PMN/1200 °C/3 h	90	− 8
(2) Stoichiometric PMN/1200 °C/1 h	96	− 4
(3) PMN–0.06MgO/1200 °C/1 h	100	− 4
(4) 0.6PMN–0.4PT–0.06MgO/1200 °C/3 h	100	− 4
(5) 0.6PZN–0.4PT–0.06ZnO/1100 °C/3 h	84	− 4

TABLE III Ratios Mg/Nb, Zn/Nb, Ti/Nb and Pb/Nb from WDS analysis for perovskite and pyrochlore phases in (a) stoichiometric PMN samples, (b) 0.6PZN–0.4PT–0.06ZnO sample

		Mg/Nb	Pb/Nb	Zn/Nb	Ti/Nb
(a)	Perovskite	0.48	1.65	–	–
	Pyrochlore	0.19	1.21	–	–
(b)	Perovskite	–	2.48	0.50	0.90
	Pyrochlore	–	1.31	0.11	0.37

(Table II), this suggests that excess MgO prevents the formation of pyrochlore phase (Reaction 1) by diffusion of Mg^{2+} into Pb^{2+} vacant sites of the perovskite structure. If fact, it seems reasonable to propose that some magnesium ions can enter A-sites in perovskite, by considering for instance, the solubility of $MgTiO_3$ in $BaTiO_3$ according to the BaO–MgO–TiO_2 phase diagram [27].

Quantitative analysis of the perovskite phase by WDS did not allow confirmation of this mechanism because of a lack of sensitivity and accuracy with respect to magnesium. The compositions of the perovskite phase obtained by this technique for Samples 3 and 4 are, respectively, $Pb_{1.04\pm0.02}Mg_{0.3\pm0.03}Nb_{0.66\pm0.02}O_3$ and $Pb_{1.02\pm0.01}Mg_{0.15\pm0.01}Nb_{0.39\pm0.01}Ti_{0.42\pm0.01}O_3$. However, a better understanding of the phase transformation from perovskite to pyrochlore was supplied by a systematic EDS study of inclusion morphology in samples 3 and 4. In both cases, EDS analysis reveals MgO particles, the number and the size of which increases from the centre to the surface of the sample, despite the absence of any pyrochlore phase. The small particles, about 100 nm in size, are included within the perovskite grains (Fig. 3). This observation is in agreement with those reported by Goo *et al.* on the distribution of MgO in PMN materials [25]. Moreover, for 0.6PMN–0.4PT–0.06MgO (sample 4), EDS analysis indicates that the composition of the largest particles near the surface is Mg_2TiO_4 (Fig. 4) compared to pure MgO in the case of small particles detected in the centre of the sample. This suggests that MgO particles correspond to residual MgO excess while Mg_2TiO_4 particles result from the transformation of the perovskite phase due to lead oxide loss near the surface at high temperature. In addition, this suggests that a progressive transformation of the perovskite phase with simultaneous precipitation of MgO (sample 3) and TiO_2 (sample 4) preceeds the formation of the pyrochlore phase.

3.2.3. PZN type sample with excess ZnO

A relatively large amount of pyrochlore phase is present near the surface of 0.6PZN–0.4PT–0.06ZnO sample. The pyrochlore grains, about 10 μm in size, have a distinctive octahedral morphology (Fig. 5a), as previously reported by Chen and Harmer for PMN ceramics [13]. The composition of the pyrochlore phase determined by WDS analysis is $Pb_{1.75\pm0.08}Zn_{0.15\pm0.05}Nb_{1.34\pm0.01}Ti_{0.5\pm0.06}O_{6.25\pm0.16}$. Then the pyrochlore phase is PbO-, ZnO- and TiO_2-deficient,

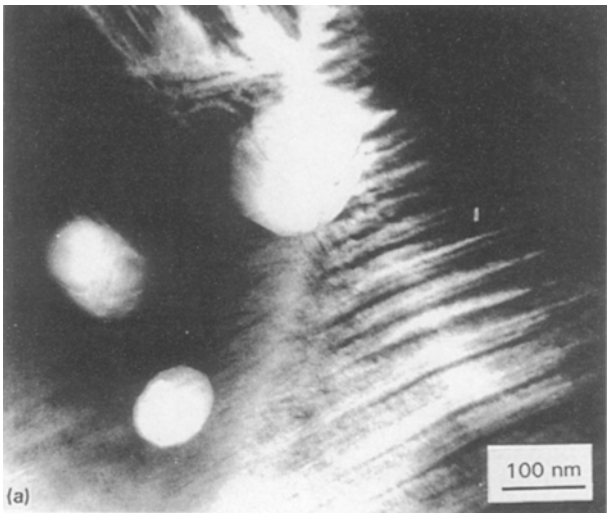

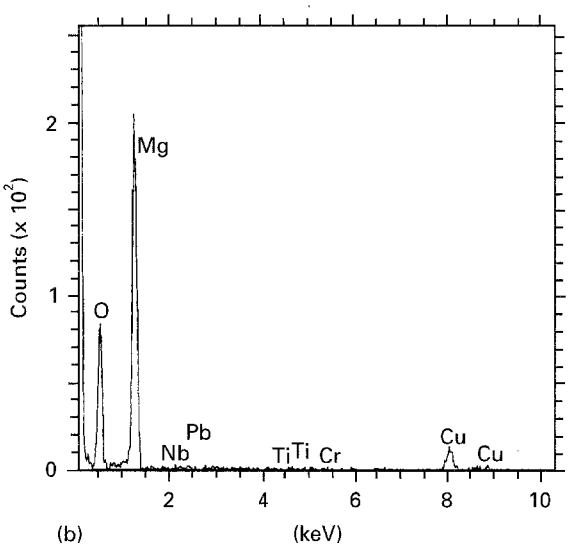

Figure 3 (a) TEM image showing submicrometre MgO inclusions in perovskite grains, (b) X-ray microanalysis spectrum from MgO particles of (a).

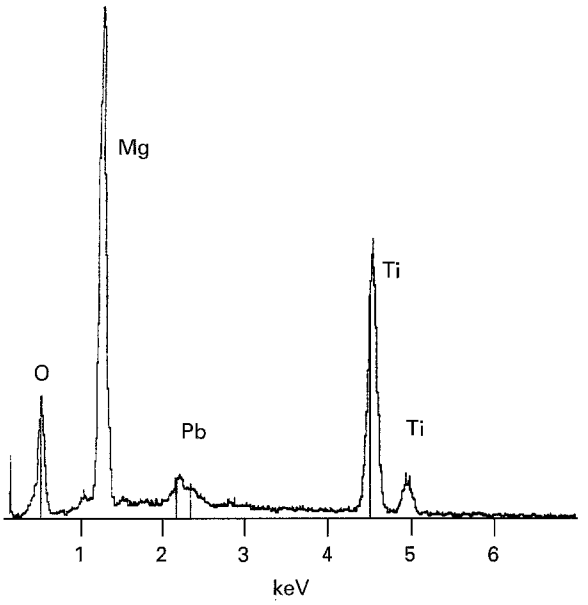

Figure 4 Energy-dispersive X-ray spectrum from Mg_2TiO_4 particle identified near the surface of the polished cross-section of 0.6PMN–0.4PT–0.06MgO (sample 4).

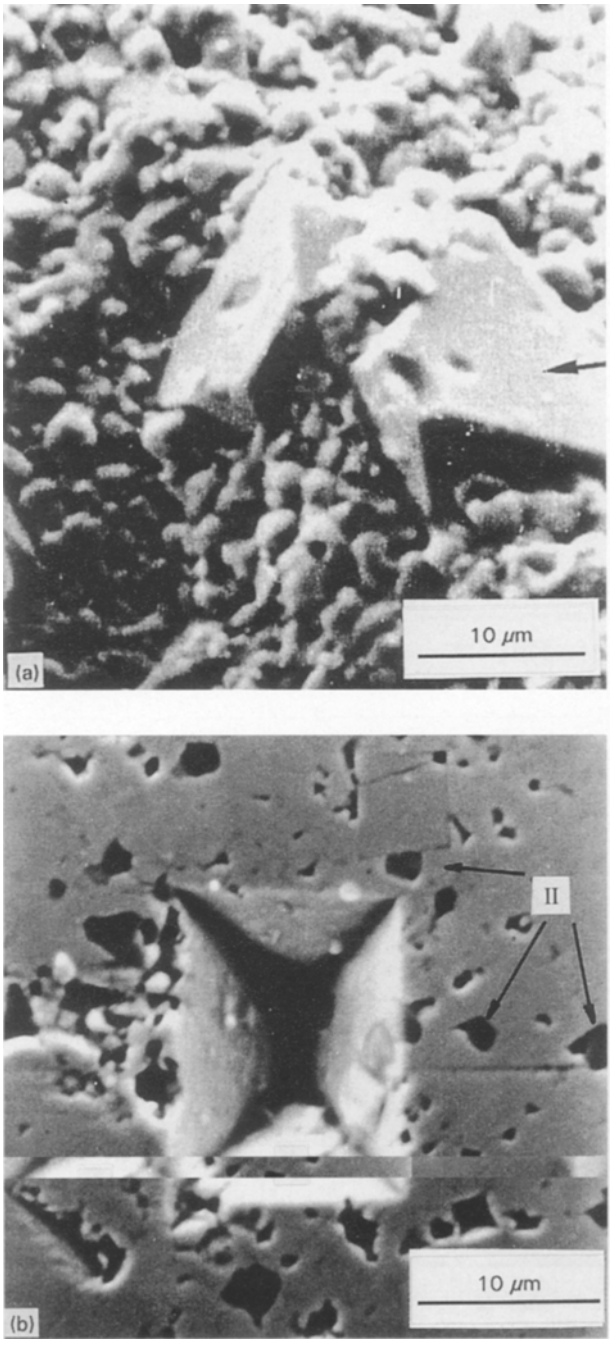

Figure 5 SEM images of 0.6PZN–0.4PT–0.06ZnO (sample 5): (a) fracture surface showing the octahedral morphology of the pyrochlore grains, (b) polished section showing the place of a pyrochlore grain (I) surrounded by ZnO and mixed ZnO–TiO_2 inclusions (II)

by comparison to the perovskite phase identified in the centre of the sample ($Pb_{0.99\pm0.05}Zn_{0.2\pm0.02}Nb_{0.4\pm0.01}Ti_{0.36\pm0.01}O_3$) (Table III). The pyrochlore is surrounded by large ZnO or mixed ZnO/TiO_2 inclusions such as Zn_2TiO_4 or $ZnTiO_3$ (Fig. 5b). This is in agreement with the corresponding ZnO and TiO_2 deficiency of pyrochlore phase.

As the 0.6PZN–0.4PT–0.06ZnO sample possesses the same PbO deficiency (-4 mol%) as the 0.6PMN–0.4PT–0.06MgO sample examined previously, it becomes obvious that a ZnO excess does not prevent the formation of a pyrochlore phase. This could be related to the poor affinity of Zn^{2+} for the perovskite A-sites. Addition of excess ZnO to the starting materials does not delay the perovskite to pyrochlore transformation by diffusion of Zn^{2+} on the Pb^{2+} vacant sites.

3.3. Reaction sequences of perovskite to pyrochlore transformation

A plausible perovskite to pyrochlore mechanism can be proposed from the different results provided by XRD, EDS and WDS analysis. The reaction sequence is governed by PbO loss which is assumed to create lead- and oxygen-site vacancies in the lattice.

3.3.1. Stoichiometric PMN system

Different reaction sequences occur in conjunction with PbO losses.

Stage I: after limited PbO volatilization, the perovskite structure remains stable and the composition is given by $Pb_{1-x}Mg_{0.33}Nb_{0.67}O_{3-x}$

Stage II: when the vacancy concentration $x/3$ on anionic sites increases, these defects are compensated through substitution of magnesium by niobium on perovskite B-sites, which leads to precipitation of MgO particles. The composition of the material can be defined as perovskite $Pb_{1-x}Mg_{0.33-\alpha}Nb_{0.66+\beta}O_3$ + MgO (inclusions) with $\beta = 2(x+\alpha)/5$ and $\alpha > 2x/3$. This explains the increasing number and size of MgO particles from the centre to the surface in samples 1 and 2.

Stage III: after larger PbO loss, i.e. for larger values of x and α, the perovskite structure of the compound $Pb_{1-x}Mg_{0.33-\alpha}Nb_{0.66+\beta}O_3$ becomes less stable than the corresponding pyrochlore. Therefore, a pyrochlore phase appears with composition $Pb_2Mg_{0.33}Nb_{1.66}O_{6.52}$, and coexists in the material with large MgO particles. This reaction sequence allows us to define the composition of the perovskite phase at its stability limit as $Pb_{0.92}Mg_{0.15}Nb_{0.76}O_3$.

3.3.2. The effect of excess MgO

After a similar stage I, the second mechanism previously identified (stage II) is delayed by the diffusion of Mg^{2+} into vacant lead-sites (stage I'), which leads to the following composition.

perovskite + inclusions (residual MgO excess)

$$(Pb_{1-x}Mg_{\delta})Mg_{0.33}Nb_{0.66}O_{3-x+\delta} + (0.06-\delta)MgO$$

The residual excess MgO corresponds to the small-size MgO particles identified in the centre of sample 3. However, as the diffusion of Mg^{2+} in perovskite structure is too slow to compensate the PbO loss, the same mechanism as in stage II in stoichiometric PMN samples prevails when the concentration of lead and oxygen reaches a critical value. This involves the precipitation of MgO inclusions in the perovskite phase $Pb_{1-x}Mg_{0.33-\alpha}Nb_{0.66+\beta}O_3$. The large MgO particles near the surface of sample 3 without any trace of pyrochlore phase result from this process.

TABLE IV Schematic phase distribution in (a) 0.6PMN–0.4PT–0.06MgO (sample 4) (b) 0.6PZN–0.4PT–0.06ZnO (sample 5)

	Pyrochlore phase	Perovskite phase	Inclusions
(a) Centre		$PbMg_{0.2}Nb_{0.4}Ti_{0.4}O_3$	0.06MgO ↑ Small size ↓
Middle area		$Pb_{1-x}Mg_{0.2}Nb_{0.4}Ti_{0.4}O_{3-x}$	0.06MgO
↓		$(Pb_{1-x}Mg_{\delta})Mg_{0.2}Nb_{0.4}Ti_{0.4}O_{3-x+\delta}$	(0.06-δ)MgO Very small size
Surface		$Pb_{1-x}Mg_{0.2-\alpha}Nb_{0.4+\beta}Ti_{0.4-\chi}O_3$	Mg_2TiO_4 large size
(b) Centre		$PbZn_{0.2}Nb_{0.4}Ti_{0.4}O_3$	0.06ZnO ↑ Small size ↓
Middle area		$Pb_{1-x}Zn_{0.2}Nb_{0.4}Ti_{0.4}O_{3-x}$	0.06ZnO
↓		$Pb_{1-x}Zn_{0.2-\alpha}Nb_{0.4+\beta}Ti_{0.4-\chi}O_3$	ZnO/TiO_2 small size
Surface	$Pb_{1.75}Zn_{0.15}Nb_{1.34}Ti_{0.5}O_{6.25}$		ZnO and mixed ZnO/TiO_2 large size

3.3.3. 0.6PMN–0.4PT–0.06MgO system

Perovskite transformation mechanisms resulting from PbO loss are similar to those described for the PMN–0.06MgO system for stages I and I′. During stage II, the oxygen-site vacancies are compensated by substitution of magnesiums and titaniums on perovskite B-sites by niobiums. This leads to the precipitation of Mg_2TiO_4 particles identified previously.

These different mechanisms are illustrated in Table IV by the distribution of phases in a cross-section of 0.6PMN–0.4PT–0.06MgO sample.

3.3.4. 0.6PZN–0.4PT–0.06ZnO system

Compared to the previous system, owing to the lack of diffusion of Zn^{2+} into lead- free A-site vacancies, stage I′ cannot be observed. Therefore, the microstructural evolution is the same as in stoichiometric PMN. This leads to the phase distribution summarized in Table IV.

4. Conclusions

1. The better stability of PMN containing an excess of MgO (0.06 mol%) is confirmed. An equivalent excess of ZnO in PZN does not prevent the formation of a significant amount of the parasitic pyrochlore phase, even after a moderate PbO loss during sintering (≈ 4 mol%).

2. The composition of the pyrochlore which coexists with the perovskite phase in PMN ceramics is $Pb_{0.92}Mg_{0.15}Nb_{0.76}O_3$, close to $Pb_6MgNb_5O_{19.5}$.

3. The microstructural evolution of the PMN samples containing an excess of MgO suggests that the apparition of the pyrochlore phase is delayed by a partial insertion of this MgO excess into the lattice vacancies created by the PbO loss at high temperature. In the case of PZN containing an equivalent excess of ZnO, the same mechanism does not operate, probably because Zn^{2+} cations are much more difficult to incorporate on the twelve-coordinated A sites of the perovskite structure.

4. In MgO-rich PMN samples, the PbO loss is nevertheless faster than the long-range diffusion of magnesia from the second phase to the perovskite matrix. The vacancies could then be compensated through an enrichment of B-sites by niobium, while now the magnesia exsolves as a (new) second phase.

5. The mictrostructural evolution of the solid solution 0.6PZN–0.4PT–0.06ZnO is similar to that of stoichiometric PMN. The ZnO-rich second phase belongs to the system $ZnO–TiO_2$,

6. On the other hand, the solid solution 0.6PMN–0.4PT–0.06MgO exhibits a good thermal stability. After PbO loss, the material contains Mg_2TiO_4 particles dispersed within a perovskite matrix.

References

1. O.FURUKAWA, M. HARATA, Y. YAMASHITA, K. INAGAKI and S. MUKAEDA, *J. Appl. Phys. supp* **26–2** (1987) 34.
2. M. S. H. CHU, in "American Ceramic Society Meeting", Cincinnati, May 1985.
3. J. M. WHEELER, UK pat. 2155006 A, 18 September 1985, Standard telephones and cables, PLC, London, UK.
4. J. KUWATA, K. UCHINO and S. NOMURA, *J. J. Appl. Phys.* **19** (1980) 2099.
5. S. NOMURA and K. UCHINO, *Ferroelectrics* **41** (1982) 117.
6. L. E. CROSS, S. J. JANG, R. E. NEWNHAM, S. NOMURA and K. UCHINO, *ibid.* **23** (1980) 187.
7. H. OUCHI, K. NAGANO and S. HAYAKAWA, *J. Am. Ceram. Soc.* **48** (1965) 630.
8. H. OUCHI, *ibid.* **51** (1968) 169.
9. F. BOSSLER, P. ESCURE, M. LEJEUNE and J. P. MERCURIO, *Ferroelectrics* **138** (1993) 103.
10. F. BOSSLER, P. ESCURE and M. LEJEUNE, *Silicates Ind.* **9–10** (1993) 181.

11. P. ESCURE, These de l'Université de Limoges, France, March 1993.
12. S. TAKAHASHI, A. OCHI, M. YONEZAWA, T. YANO, T. HAMATSUKI and I. FUKUI, *Ferroelectrics* **50** (1983) 181.
13. J. CHEN and M. P. HARMER, *J. Am. Ceram. Soc.* **73** (1990) 68.
14. J. P. BOILOT, O. BOUQUIN and M. LEJEUNE, *Silicates Ind.* **1–2** (1990) 27.
15. O. BOUQUIN, M. LEJEUNE and J. P. BOILOT, *J. Am. Ceram. Soc.* **74** (991) 1152.
16. S. L. SWARTZ, T. R. SHROUT, W. A. SCHULZE and L. E. CROSS, *ibid.* **67** (1984) 311.
17. H. C. WANG and W. A. SCHULZE, *ibid.* **73** (1990) 825.
18. O. FURUKAWA, Y. YAMASHITA, M. HARATA, T. TAKAHASHI and K. INAGAKI., *J. J. Appl. Phys. supp* **24–3** (1985) 96.
19. A. HALLIYAL, T.R. GURUJA, U. KUMAR and A. SAFARI, in "Proceedings of IEEE International Symposium on Application of Ferroelectrics", Bethlehem, PA (1986).
20. J. R. BELSICK, A. HALLIYAL, U. KUMAR and R. E. NEWNHAM, *Am. Ceram. Soc. Bull.* **66** (1987) 664.
21. S. Y. CHEN, S. Y. CHENG and C. M. WANG, *J. Am. Ceram. Soc.* **74** (1987) 664.
22. Y. MATSUO, H. SASAKI, S. HAYAKAWA, F. KANAMARU and M. KOIZUMI, *ibid.* **52** (1969) 516.
23. I. I. ADRIANOVA, A. A. BEREZHNOI, E. V. NEFEDOVA, V. A. PISMENNYI, V. POPOV and K. P. SKORNYAKOVA, *Opt. Spectrosc.* **36** (1974) 547.
24. S. L. SWARTZ, T. R. SHROUT, W. A. SCHULZE and L. E. CROSS, *J. Am. Ceram. Soc.* **68** (1985) C87.
25. E. GOO, T. YAMAMOTO, and K. OKAZAKI, *ibid.* **69** (1986) C188.
26. S. K. SAHA and D. C. AGRAWAL, *Bull. Am. Ceram. Soc.* **71** (1992) 1424.
27. R. S. ROTH, W. S. BROWER, M. AUSTIN and M. KOOB, National Bureau of Standards (US) Internal Report, NB-SIR 81-2441 (1981) pp. 42.

Received 20 September 1995
and accepted 15 January 1996